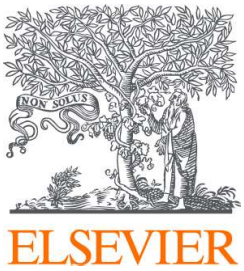

Sensors & Actuators: B. Chemical 377 (2023) 133052

Contents lists available at ScienceDirect

Sensors and Actuators: B. Chemical

journal homepage: www.elsevier.com/locate/snb

Peptide-based direct electrochemical detection of receptor binding domains of SARS-CoV-2 spike protein in pristine samples

T.H. Vignesh Kumar [a,1], Sowmiya Srinivasan [b,2], Vinoth Krishnan [a,c,2], Rama Vaidyanathan [b,d], Kannadasan Anand Babu [b,*], Sudhakar Natarajan [e,*], Murugan Veerapandian [a,c,**]

[a] Electrodics and Electrocatalysis Division, CSIR-Central Electrochemical Research Institute (CECRI), Karaikudi 630003, Tamil Nadu, India
[b] Dr. A.P.J. Abdul Kalam Center of Excellence in Innovation and Entrepreneurship, Dr. M.G.R. Educational and Research Institute, Chennai 600095, Tamil Nadu, India
[c] Academy of Scientific and Innovative Research (AcSIR), Ghaziabad 201002, India
[d] Department of Biotechnology, Dr. M.G.R. Educational and Research Institute, Chennai 600095, Tamil Nadu, India
[e] Department of Virology and Biotechnology, ICMR-National Institute for Research in Tuberculosis, Chennai 600031, Tamil Nadu, India

ARTICLE INFO

Keywords:
N-terminal *h*ACE-2 peptide
SARS-CoV-2 RBD
Peptide biosensor
RNA Isolation-free
Electrochemical biosensor
COVID sensor

ABSTRACT

RNA isolation and amplification-free user-friendly detection of SARS-CoV-2 is the need of hour especially at resource limited settings. Herein, we devised the peptides of human angiotensin converting enzyme-2 (*h*ACE-2) as bioreceptor at electrode interface for selective targeting of receptor binding domains (RBD) of SARS-CoV-2 spike protein (SP). Disposable carbon-screen printed electrode modified with methylene blue (MB) electro-adsorbed graphene oxide (GO) has been constructed as cost-efficient and scalable platform for *h*ACE-2 peptide-based SARS-CoV-2 detection. *In silico* molecular docking of customized 25 mer peptides with RBD of SARS-CoV-2 SP were validated by AutoDock CrankPep. N-terminal region of ACE-2 showed higher binding affinity of − 20.6 kcal/mol with 15 H-bond, 9 of which were < 3 Å. Electrochemical biosensing of different concentrations of SPs were determined by cyclic voltammetry (CV) and chronoamperometry (CA), enabling a limit of detection (LOD) of 0.58 pg/mL and 0.71 pg/mL, respectively. MB-GO devised *h*ACE-2 peptide platform exert an enhanced current sensitivity of 0.0105 mA/pg mL^{-1} cm^{-2} ($R^2 = 0.9792$) (CV) and 0.45 nA/pg mL^{-1} ($R^2 = 0.9570$) (CA) against SP in the range of 1 pg/mL to 1 μg/mL. For clinical feasibility, nasopharyngeal and oropharyngeal swab specimens in viral transport medium were directly tested with the prepared peptide biosensor and validated with RT-PCR, promising for point-of-need analysis.

1. Introduction

Rapid spread of severe acute respiratory syndrome coronavirus 2 (SARS-CoV-2) with > 516 million cases and nearly 6.25 million fatality as per May 2022 report, COVID-19 made global lives with an ever-growing burden [1]. The nucleotide sequences of SARS-CoV-2 are 79% identical to those of 2003 SARS-CoV-1 [2]. SARS-CoV-2 is spherical with a diameter of 50–100 nm having lipid membranous envelop around the viral RNA. The four basic structural proteins of SARS-CoV-2 are the spike (S), membrane (M), envelope (E), nucleocapsid (N) proteins [3]. The proteins binding to the host cell receptor of *h*ACE-2, allow the viral RNA entry. The two sub-domains of S-protein (S1 and S2) play a prime role in the host interaction [4]. The RBD of the S2 is responsible for the ACE2 link. Incorporation of viral RNA into the host cell membrane is also made easier by the S1 domain [4]. The SARS-CoV-2 virus, on the other hand, is more contagious and spreads faster than SARS-CoV-1. As a result, the virus spreads quickly through contact, droplet, blood, fecal-oral, airborne, and fomite transmission methods [5]. Cough, shortness of breath, diarrhea, and fever are some of the common symptoms among persons affected with COVID-19 disease [2]. During the incubation phase, the infected person is very contagious and can transmit the virus to others [6]. Thus, rapid detection of COVID-19 is

* Corresponding authors.
** Corresponding author at: Electrodics and Electrocatalysis Division, CSIR-Central Electrochemical Research Institute (CECRI), Karaikudi 630003, Tamil Nadu, India.
E-mail addresses: kabpharm@gmail.com (K.A. Babu), sudhakar.na@icmr.gov.in (S. Natarajan), vmurugan@cecri.res.in (M. Veerapandian).
[1] Present address: Electrical and Computer Engineering, Iowa State University, Ames, IA 50011, United States.
[2] Equally contributed.

https://doi.org/10.1016/j.snb.2022.133052
Received 24 July 2022; Received in revised form 22 November 2022; Accepted 23 November 2022
Available online 23 November 2022

essential for containment of disease spread and early clinical care.

COVID-19 tests have been expanded to detect social breakouts, although they are fraught with difficulties. Frontline diagnostic methods for COVID-19 screening includes RT-PCR, which is superior in sensitivity and selectivity than nucleic acid hybridization procedures. RT-PCR often demands 24 hrs to declare the results, involving sample collection, transport, viral RNA preparation and analysis [7]. Moreover, skilled manpower and sophisticated equipment are mandate [8]. Second common clinical diagnosis is based on chest CT scan with an 87.9% confidence level, SARS-CoV-2 findings in thoracic CT images include ground-glass opacity (GGO), crazy-paving and consolidation, reverse halo, air bronchograms, and perilobular pattern [9–11]. CT scans, on the other hand, raise the risk of radiation and are expensive than nucleic acid-based testing [2,8]. Although the serological antigen tests are rapid relatively affordable and has a short turnaround time, still not sensitive as nucleic acid testing [8,12,13]. Antibody tests, on the other hand, has limitations to survey the seroprevalence against to SARS- CoV-2 in population [8].

Electrochemical biosensors based on disposable screen-printed electrode (SPE) has merits suitable for point-of-care analysis, due to its rapid analytical response time, high sensitivity even with ultra-low concentration and user-friendly operation [14]. Nevertheless, effective electrochemical biosensor design is highly tricky, mainly achieving durable redox behavior at complex analyte environment without compromising compatibility against the suitable bioreceptors. To enable cost-efficient design significant interests were devoted on the development of carbon-based nanomaterials including nanotubes, nanosheets and quantum dots. Amongst, existence of abundant surface functional groups, scalable syntheses process and tunable electrochemical active surface coverage made layered graphene derivatives as potential sensor material for various biomarker sensing [15–18].

Besides electrochemical active surface area, selective bio-receptors are vital need for the detection of surface proteins of virus irrespective of the source of test samples. The RBD in the spike proteins of SARS-CoV-2 has a greater affinity for the *h*ACE-2 than SARS-CoV-1, according to structural modeling and atomic-level imaging investigations [19–21]. *In silico* studies for the design of peptide regions of *h*ACE-2 suitable for binding the RBD of spike protein in SARS-CoV-2 have been recently reported [22–27]. Zhu and Zhou have designed a colorimetric sandwich type SARS-CoV-2 bioassay using specific peptides modified gold nanoparticles (AuNPs) exhibiting a LOD of 0.26 ng/mL. While promising, the detection limits of these colorimetric sensors are far from the sub-pg/mL values desired by clinical community and are often achievable by more advanced but expensive CT scan and RT-PCR methods [7,10]. To the best of authors knowledge there are no report customizing peptides as bioreceptor to electrochemically probe the SP of SARS-CoV-2. Therefore, in this work an attempt was made to develop electrochemical oligopeptide-based biosensor platform devising shortest functional oligopeptides of N-terminal RBD-*h*ACE-2 for detection/determination of SARS-CoV-2 SP. Distinctly a sensor element comprising layered nanostructures of graphene oxide (GO) and electroadsorbed methylene blue (MB) were devised. With suitable activation layer, MB-functionalized GO electrode surface (MB-GO) enable efficient loading of bioreceptor, N-terminal *h*ACE-2 peptide, and exert selective/specific targeting of SARS-CoV-2 spike protein (SP), regardless of common interferents circumventing the nucleic acid amplification step (Scheme S1). As we show below, the SPE, planar device achieves a sensitivity of 0.0105 mA/pg mL^{-1} cm^{-2} in CV and 0.45 nA/pg mL^{-1} in CA of SARS-CoV-2 for a small working electrode size (2 mm). Compared to colorimetric approach using similar *h*ACE-2 bioreceptor, the electrochemical method of analysis exhibits a better LOD (three order of magnitude) of 0.58 and 0.71 pg/mL from CV and CA, respectively. Further, the diagnostic feasibility of oligopeptide biosensor was tested with gargled-lavage samples containing artificially spiked target analytes. For clinical validation oro-/-naso-pharyngeal swab samples were utilized and demonstrated for qualitative and quantitative discrimination of the target SARS-CoV-2 SP, promising for point-of-need analysis.

2. Experimental procedures

2.1. Fabrication of electrochemical peptide sensor platform

A carbon-based screen-printed electrode (SPE) from Pine research instrumentation, NC, USA, containing an integrated carbon as working (2 mm diameter) and counter electrode (U-shaped), with the circular-shaped Ag/AgCl as reference electrode was used as base for sensor construction. After a gentle rinse with 10 mM PBS buffer (pH 7.4), an aqueous dispersion of MB-GO (6 μL) was drop casted and incubated for 30 min at room temperature (RT) to achieve a monotonous layer on the working electrode surface. 4 μL of Nafion was used as binder on the MB-GO/SPE. Pristine GO and MB was also prepared on SPE for control studies. A stepwise protocol for preparing electrode ink is detailed in supplementary information (Fig. S1). The concentration of precursors used in electrode ink formulation are as follows: MB-GO (0.16 mg/mL GO in 1 mM MB); GO dispersion (0.16 mg/mL); MB (1 mM) solution.

Before processing the peptide immobilization, a bioaffinity layer (*b*) from AnteoBind™ (4 μL) was drop casted on the MB-GO/SPE and allowed it to dry for 30 min. By drop casting, 6 μL of N-terminal peptides (NPs) (0.1 mg/mL) on the activated surface of *b*/MB-GO/SPE and incubated at room temperature for 30 min. The surplus electrode materials on the surface were gently removed by immersing for 2 s in a PBS solution [28–32] To avoid non-specific bindings, the electrode was treated with bovine serum albumin (BSA) solution (4 μL, 0.05 mg/mL). After rinsing with PBS buffer for 2 s, the prepared BSA/NP/*b*/MB--GO/SPE sensor platform was demonstrated for probing SARS-CoV-2 SP antigen [33–35].

2.2. Peptide detection of SARS-CoV-2 SP antigen

A stock solution of SARS-CoV-2 SP (0.1 mg/mL) was prepared by Milli-Q water with 50% glycerol solution, and kept at − 20 °C. From this stock, desired amounts of analyte solutions were processed as test samples. A 4 μL of target SARS-CoV-2 SP with different concentrations were placed on the individual peptide sensor surface and 20 min incubated at RT. Electrochemical peptide sensing measurements were performed on as-incubated electrodes utilizing CV and CA methods. Triplicates of all electrode preparations and electrochemical measurements were performed. Due to the lower standard deviation (SD) of the triplicate answer, some of the error bars may not be visible in the graph.

3. Results and discussion

3.1. Molecular docking and interaction analysis of SARS CoV-2 spike protein with hACE-2 peptides

Both the N-terminal and C-terminal peptide were docked in the active site of SARS CoV-2 spike protein to identify the high binding affinity peptide of *h*ACE-2. The active site residues include K417, G446, Y449, N487, Y489, Q493, T500, N501, G502 and Y505 in the RBD of SARS CoV-2 spike protein. The highest negative docking pose was analysed for high binding affinity peptide. The docked structure was analysed for hydrogen bond and hydrophobic interactions (Table S1). From the interaction plot, it can be inferred that N-terminal peptide has high binding affinity towards spike protein than C-terminal observed from the strength of the H-bonds formed (Fig. 1A-B), (Figs. S2 and S3) and (Tables S2 and S3). From the docking results of the *h*ACE-2 peptides, we have commercially synthesized the peptides.

3.2. Characterization of the peptides

The secondary structure of the commercially synthesized peptide was analysed by circular dichroism (CD) spectroscopy. By

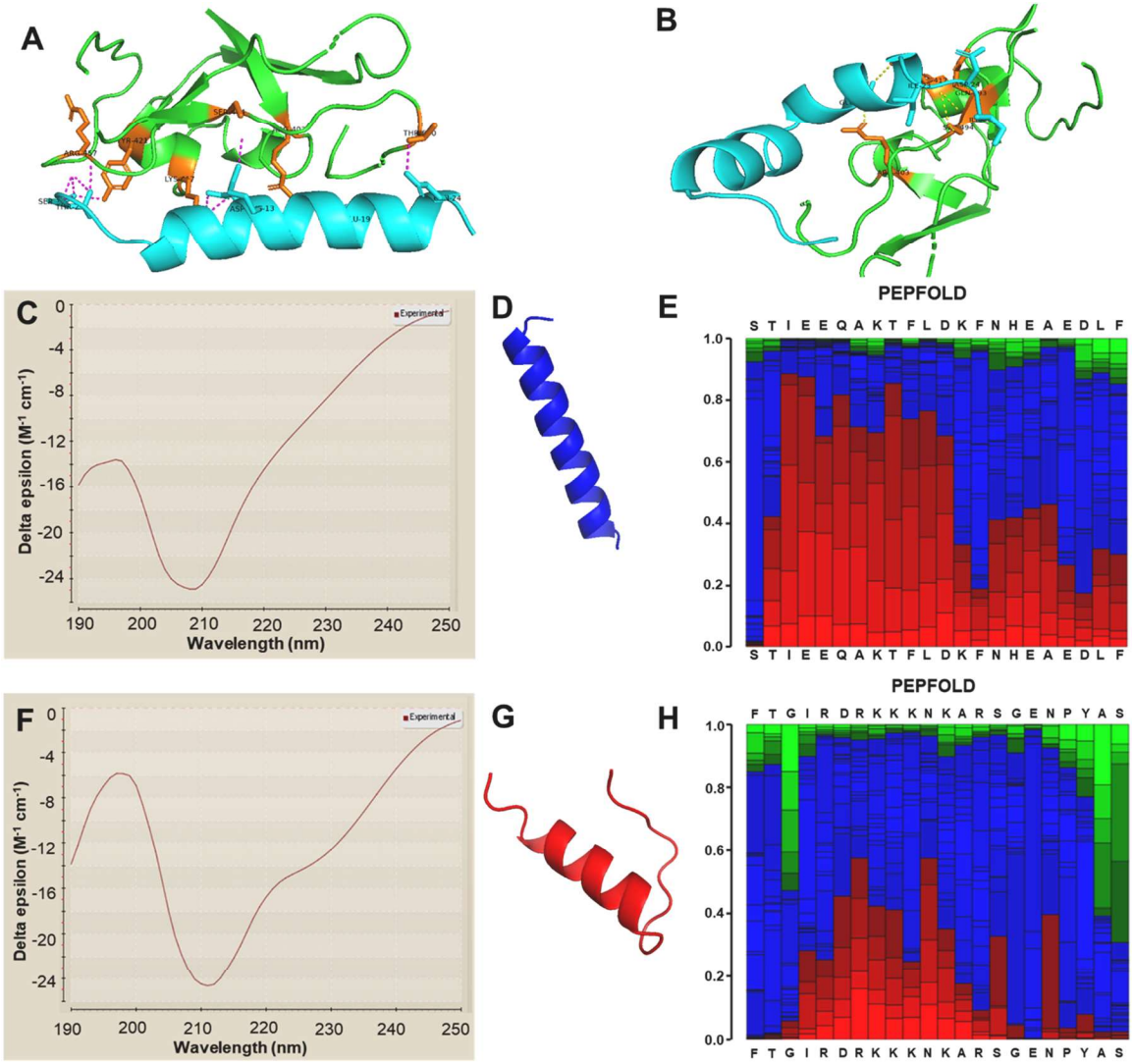

Fig. 1. Comparison of *h*ACE-2 N-terminal and C-terminal peptides. Binding profile of *h*ACE-2 peptides (cyan) and SARS CoV-2 spike protein (green and orange {interacting amino acid residues}). (A) N-terminal peptide, (B) C-terminal peptide. Circular Dichroism spectrum of (C) N-terminal peptide and (D) its secondary structure (STIEEQAKTFLDKFNHEAEDLFYQ) predicted by PEP-FOLD 3.5 server. (E) Secondary structure contents in the predicted structure of N-terminal peptide, composed of 71.4% α-helix (red), 28.5% coil (blue) and no extended (green) structure. (F) C-terminal peptide and (G) predicted secondary structure (FTGIRDRKKKNKARSGENPYASIDI). (H) Secondary structure contents in the predicted structure of C-terminal peptide, composed of 31.8% α-helix (red), 54.5% coil (blue) and 13.6% extended (green) structure.

deconvoluting the spectrum using BeStSel server, the secondary structure content of N-terminal peptide such as α-helix, antiparallel β-sheets, parallel β-sheets and other including random coil/loop was found to be 39.2%, 31.1%, 3.7% and 25.9%, respectively. While the C-terminal peptide has 36.9% α-helix, 24.2% antiparallel β-sheets, 13.3% parallel β-sheets and 25.6% of other structures (Fig. 1C-F). Likewise, the secondary structure of N- and C-terminal peptides were also predicted using PEP-FOLD 3.5 server. From which the predominant α-helix structure in the N- and C-terminal region was found to be 71.4% and 31.8%, respectively. Though, it has variations compared to CD spectra still it is in agreement with earlier report [36] (Fig. 1 D, E, G and H). Thus, based on the abundant existence of α-helix structure in the N-terminal region and specificity toward the target RBD of SP, in this work the N-terminal peptide regions are customized as bioreceptor on the electrode interface.

3.3. Physico-chemical characterization

The surface morphologies of the GO and MB-GO sheets were examined using FE-SEM (Fig. S4). The GO was in the shape of a randomly aggregated flaky texture with a partly curled edge, and the sheets were micrometer scale in size Fig. S4 (A) [37,38] The morphology of MB-GO, on the other hand, was noticeably different. The surface of MB-GO sheets was significantly more rippled than that of GO sheets, showing that MB molecules were effectively interacted with GO, length and thickness of GO sheets were also enhanced due to the π-π interactions of the conjugated molecular systems (Fig. S4 (B)) [37,38] The elemental analysis of GO and MB-GO was also performed using EDS spectra. The presented elements (C, O in GO) and (C, N, S in MB-GO) from the obtained spectra was clearly indicated that MB is functionalized with GO (Fig. S4 (C-D)).

The creation of the MB-GO microstructure was investigated using UV–vis spectroscopy. Fig. S5 (a) shows the UV–vis spectra of MB, GO and MB-GO in aqueous solution. The MB molecule showed two major absorption peaks at 291 and 663 nm, and two additional shoulder peaks found at 245 and 610 nm were assigned to MB dimer in an aqueous solution [37] The GO spectrum showed one absorbance and one shoulder peak at 238 and 275 nm, which were attributed to π-π transitions (C-C) and n-π transitions (C═O), respectively [39] The absorption

peak of GO and MB was moved to 231 nm and 688 nm after the synthesis of MB-GO. The absorption band of the GO and MB in water was previously known to be around 238 nm and 663 nm. The shift was attributed to MB-GO interactions, implying that the electronic conjugation structure inside the MB-GO sheets was extended during the alteration process [37,39].

Raman spectroscopy is a nondestructive chemical analysis technique that is used to investigate the lattice network and electronic properties of GO and MB-GO sheets [35,38,40] Using a 532 nm laser, the Raman spectra of MB, GO, and MB-GO (Fig. S5 (b)) samples were recorded. C-N symmetrical stretching (1388 cm^{-1}) and C-C ring stretching were visible in the spectra of pure MB (1627 cm^{-1}) [41] Furthermore, the GO spectra exhibits four distinct peaks at 1583, 2703, 1350, and 1623 cm^{-1}, which are attributed to the G, G′, D, and D′ bands, respectively. The G and G′ bands are formed by the C-C bond stretch and are shared by all sp^2 carbon atoms in a 2D hexagonal lattice [35,42] The double resonance process activates first and second order Raman scattering, resulting in the formation of these bands. Furthermore, the occurrence of D and D′ bands is linked to lattice deformation or defects involving sp^3 carbon atoms [42] The in-plane optical branches (longitudinal and transverse modes) are responsible for both D bands. The D- and G- band of intensity ratio ($I_{(D)}/I_{(G)}$) is 0.74 [38,42] After MB changed GO peaks, the D, D′, G, and G′ bands were shifted to 1343, 1615, 1576, and 2693 cm^{-1}, respectively. The mixing of MB has a significant impact on the sp^2 graphitic carbon area on the GO, as demonstrated by a blue shift in the G-band and a drop in the $I_{(D)}/I_{(G)}$ ratio is 0.60 [38,42] According to the sonochemically generated GO-MB nanocomposite, the new moderate signal at 1453 cm^{-1} corresponds to the MB vibrational modes. These findings indicate that MB molecules that are redox active have been successfully changed on the surface of GO sheets [38].

3.4. Electrochemical study

3.4.1. Cyclic voltammetry study

Voltammetry is a quantitative method of analysis based on faradaic impedance capable of analysing single or multiple analytes from a single sample. Voltammetry is relatively simple to evaluate the solution resistance and double layer capacitance. As long as the analyte species behave independently, the resulted voltammogram could summarize the individual analyte attributed signals. The accuracy of any voltammetric analysis is often limited by the ability to correct the residual currents, particularly those due to charging. Sensing accuracy of voltammetry is especially challenging in low analyte concentration. Precision of this technique could be influenced by the uncertainty in measuring the limiting current or the peak current. Nevertheless, by optimal experimental conditions the accuracy/precision can be improved. The CV of bare SPE, MB/SPE, GO/SPE and MB-GO/SPE electrodes is shown in Fig. 2(A), which was evaluated at a 50 mV/s of scan rate in the presence of 0.1 M PBS electrolyte (pH 7.4). Under the specified experimental conditions, there is no redox behavior between the bare SPE and the GO/SPE. The GO-SPE, on the other hand, displayed a cathodic reduction peak at roughly − 0.7 V, which was attributed to GO's surface oxygen groups being reduced [43] MB/SPE have greater redox behavior than GO/SPE and bare SPE. However, pristine MB/SPE do not allow for long-term redox behavior at the interface due to physical adsorption [38]. The 1 mM MB mixed 0.16 mg/mL GO (e.g.,

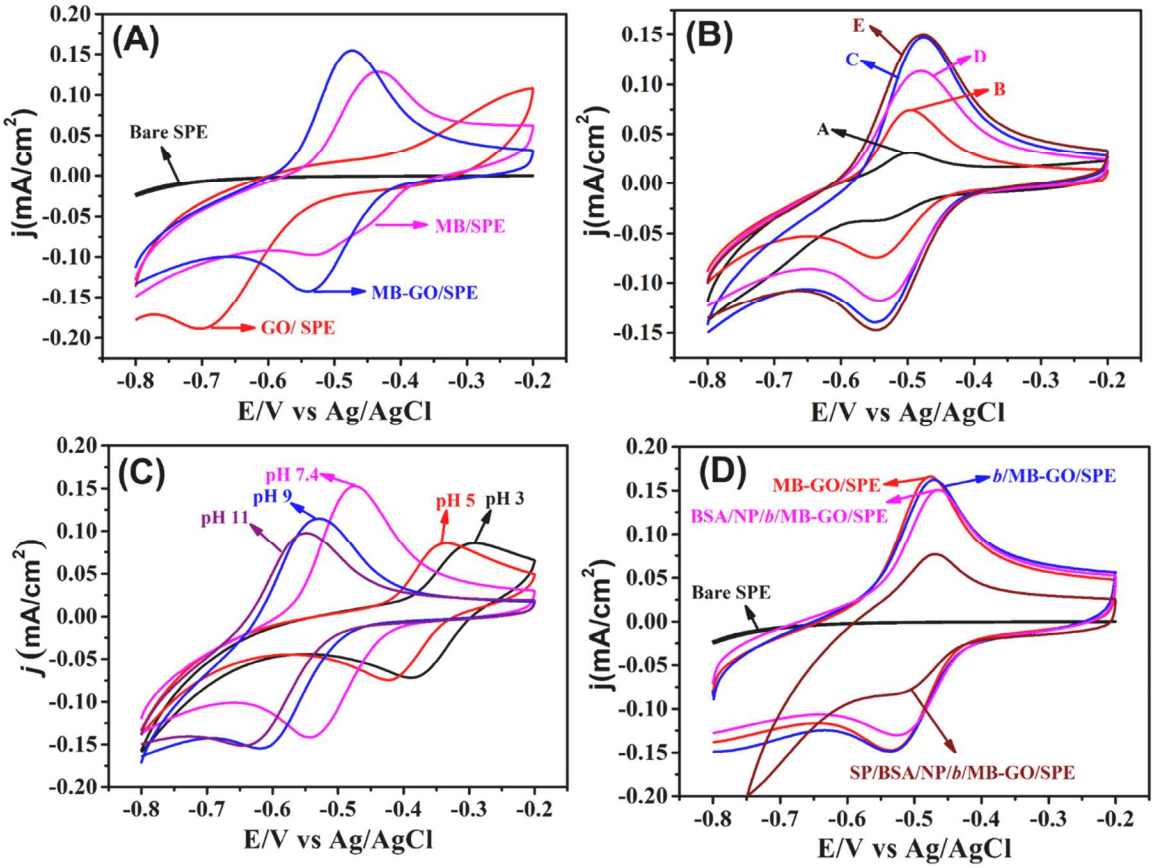

Fig. 2. (A) CVs of bare SPE, GO/SPE, MB/SPE, MB-GO/SPE recorded in 0.1 M PBS (pH 7.4) at a scan rate of 50 mV/s. (B) CVs of MB-GO/SPE with different concentrations (A to E). The catalyst concentration details: A = 0.016 mg/mL (GO) in 0.1 mM (MB), B = 0.08 mg/mL (GO) in 0.5 mM (MB), C = 0.16 mg/mL (GO) in 1 mM (MB), D = 0.25 mg/mL (GO) in 1 mM (MB), E = 0.5 mg/mL (GO) in 2 mM (MB) recorded in 0.1 M PBS (pH 7.4) at a scan rate of 50 mV/s. (C) CVs of MB-GO/SPE recorded in 0.1 M PBS with different pH conditions at a scan rate of 50 mV/s. (D) CVs of bare SPE, MB-GO/SPE, *b*/MB-GO/SPE, BSA/NP/*b*/MB-GO/SPE and SP/BSA/NP/*b*/MB-GO/SPE recorded in 0.1 M PBS (pH 7.4) at a scan rate of 50 mV/s.

MB-GO) electrode, on the other hand, exhibits reversible redox behavior with a cathodic and anodic peak potential of − 0.54 and − 0.48 V [38] The redox peak current densities of this MB-GO/SPE electrode material (I_{pa} = +0.154 mA. cm^{-2} and I_{pc} = −0.141 mA. cm^{-2}) are found to be higher than other modified electrodes examined. The MB-GO/SPE electrode's stability was then assessed using 20 repeated CV measurements (Fig. S6).

The fact that the reversible redox peak current densities remained constant as the number of scan cycles increased shows that the Nafion coatings aided in keeping the MB-GO from leaching out of the electrode surface [44]. The observed redox behavior of MB ↔ leuco-MB is quite similar to that of SPE modified with other nanomaterials (carbon nanotubes, graphene and reduced graphene oxide) mixed with MB [38, 45–47] The strong interaction between the MB and GO could potentially be due to electrostatic and π-π stacking [38] In general, the redox molecules modified electrode is determined by the protection of the electrode surface from the polymer membrane, the scan rate, and the pH of the electrolyte solution. The high surface area and oxygenated functional groups of GO is clearly helpful in the adsorption of MB in aqueous solution, as evidenced by the earlier section. The long-lasting and enhanced redox behavior of MB-GO modified electrodes is expected to be beneficial for biosensor applications [38].

Different concentrations of MB-GO modified SPE electrode to examine the effect of the amount of MB-GO modified electrode on oxidation current densities (j_{pa}) and oxidation peak potentials (E_{pa}) (Figs. 2(B) and S7(a)). The peak current density of the MB-GO/SPE electrode risedronate as the concentration increased from 0.016 mg/mL (GO) in 0.1 mM (MB) to 0.16 mg/mL (GO) in 1 mM (MB), as shown in Fig. 2(B). The peak current density of the MB-GO/SPE electrode was marginally reduced after increasing GO concentration alone in MB solution 0.25 mg/mL (GO) in 1 mM (MB). The peak potential and current density did not change significantly when the concentrations of GO and MB were 0.16 mg/mL (GO) in 1 mM (MB) and 0.5 mg/mL (GO) in 2 mM (MB), which could be owing to the outstanding synergistic impact of MB and GO [37] Therefore, 0.16 mg/mL (GO) in 1 mM (MB) was chosen for subsequent experiments.

In different pH solutions, the electrochemical activity of MB-GO/SPE was examined by CV. The corresponding MB ↔ LMB redox peak currents and potentials were recorded as shown in Fig. 2(C). A relationship between pH and MB oxidation current densities (j_{pa}) and oxidation peak potentials (E_{pa}) (Fig. S7(b)). At pH 7.4, the highest MB oxidation peak current density was found. As a result, pH 7.4 was chosen as the best pH for further investigations.

To study the scan rate effects on the anodic and cathodic peaks of MB-GO/SPE, as seen in Fig. S7(c) and (d). A quick electron transfer mechanism is demonstrated by a narrow peak potential separation with sigmoidal shape [38] Correlation co-efficient of 0.9985 (anodic current density) and 0.9763 (cathodic current density) were obtained by fitting the redox peak current densities versus scan rates. These findings imply that the MB-GO/SPE generates a surface confined redox behavior, which is favorable platform for biosensor applications. Further, electro active surface area of MB-GO/SPE was found to be 13×10^{-10} mol cm^{-2}, using the formula $\Gamma = Q/nFA$ (Figs. 2 and S7) [35]. The fabricated MB-GO hybrid material is modified into SPE, which will be applied to the peptide biosensor operating system after analysing the essential voltammetric properties.

The CV of MB-GO/SPE in 0.1 M PBS electrolyte (pH 7.4) are shown in Fig. 2(D). Continuous CVs were recorded after each surface modification to ensure that active layers of chelating agents (AnteoBind), bioreceptors (N-terminal *h*ACE-2 peptide), blocking agents (bovine serum albumin), and targets (SP protein) were immobilized on the electrode surface. The CV of bare SPE and GO/SPE does not have redox activity, however the MB-GO/SPE exhibit a redox peak (quasi-reversible) due to the transformation of MB ↔ LMB. The redox behavior of MB-GO is maintained after activation of the AnteoBind (*b*), N-terminal *h*ACE-2 peptide (NP), and bovine serum albumin (BSA) layers, with only a minor reduction in current sensitivity [33–35]. The NP is well retained by the interface of *b* on the electrode surface. The current response of the NP immobilized electrode surfaced showed a substantial decline due to its binding affinity with target SP, as seen by the CV (Figs. 2d and 3A).

The CV and chronoamperometry techniques further ensured the development of competitive peptide and protein interactions at the electrode surface. The anodic peak current density of the BSA/NP/*b*/MB-GO/SPE electrode was examined in particular for variations in analyte concentration (Fig. 3(A)). The higher anodic peak and current density (0.150 mA cm^{-2}) of BSA/NP/*b*/MB-GO/SPE electrode attributed to MB ↔ LMB in immaculate condition, as can be shown. However, when SP protein (1 pg/mL) is added, the current is reduced to 0.141 mA cm^{-2}. The reduced current density is corresponding to the SP concentration, implying that peptide and protein interactions at the interface have formed successfully. The calibration plot derived from CV study against different SP concentration (0.001, 0.01, 0.1, 1, 10, 100, 1000 ng/mL) exhibit a correlation coefficient of 0.9792 (Fig. 3(B)) and (Table S4) [48–53] The current sensitivity of the as-fabricated electrode was determined to be 0.0105 mA/pg mL^{-1} cm^{-2}. From the CV studies, the LOD for the analyte SP was calculated to be 0.58 pg/mL using the following Eq. (1) [44].

$$LOD = \frac{3SD}{m} \quad (1)$$

where, *SD* is the standard deviation of blank and *m* is the slope of the calibration curve. The calculated LOD is comparable with other similar analytical techniques (Table S5) [54–61] and convenient for even measuring the ultralow viral loads in the clinical samples [55].

Ensuring the selectivity/specificity of the sensing substrate is highly essential for any realistic application. To study the matrix effect on the prepared biosensor platform, the common viral infection-associated interferants such as non-structural protein 1 (NS1), human serum albumin (HSA) and immunoglobulin G (IgG) were utilized [35]. The CV response of the fabricated BSA/NP/*b*/MB-GO/SPE sensor against multifold concentration (100 ng/mL) of pristine interferents and mixtures of test samples containing analyte SP (100 pg/mL) and interferants are shown in Fig. 3(C-D). With activated bio-affinity layer, the immobilized bioreceptor, customized N-terminal *h*ACE-2 peptide regions, exerted better loading on the electrode surface. The residual void spaces are covered by BSA to circumvent the matrix effect and to allow the specific interaction of target SP on the bioreceptor- active sites. However, there were impaired interaction, when the target concentration (1 pg/mL) and interferant (100 pg/mL) was kept in 1:100 ratio, particularly significant in voltammogram. On the other hand, when the analyte concentration was elevated to 100 pg/mL irrespective of 1000-fold hike in interferant's concentration (i.e., 100 ng/mL), the current response from the prepared biosensor platform were distinct both in CV and CA methods. The percentage of relative standard deviation (%RSD) from the interferent analysis are furnished in Table S6.

3.4.2. Chronoamperometry (CA) study

To supplement the CV study and to test the portable configuration feasibility of the proposed platform for on-site analysis, a CA technique was investigated (Fig. 4). CA is a sensitive and straightforward technique, does not demand labeling of analyte/bioreceptor, used to measure current–time dependence according to the diffusion of analyte from the bulk to the electrode surface. Since the CA scan directly relates the sum of the faradaic currents mediated by the diffusion of ions in solution that are reduced at a potential more positive than E_a, evaluation of single analyte concentration in a solution with different molecules might be difficult. However, in-situ redox species associated signal transduction correlating the concentration gradient from the immunocomplex or nucleic acid hybridization is advantageous for target sensing. The CA response against the SP concentrations was measured at an applied bias potential of − 0.48 V attributed to the MB oxidation in the GO peptide

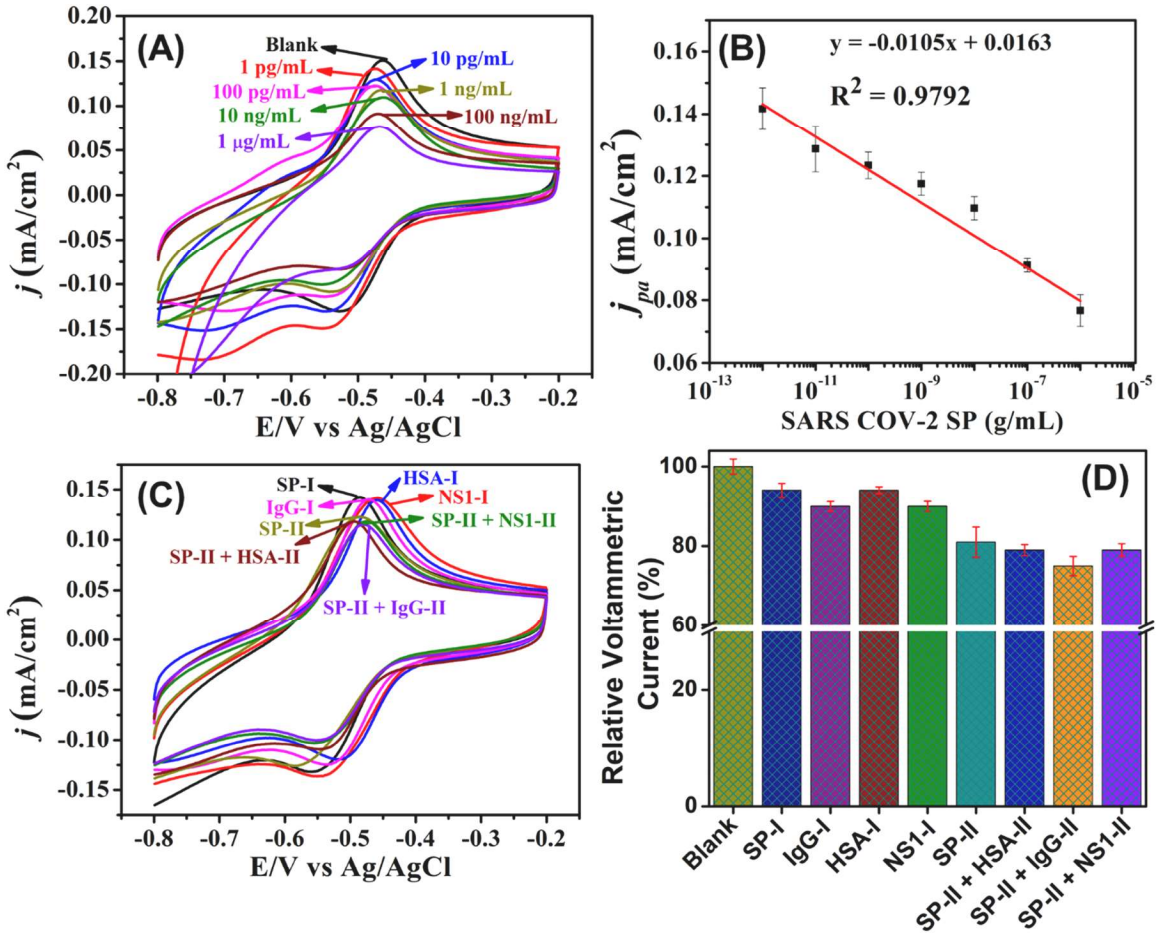

Fig. 3. (A) CV of BSA/NP/*b*/MB-GO/SPE electrodes versus various concentrations of SARS-CoV-2 SP recorded in 0.1 M PBS (pH 7.4) at a scan rate of 50 mV/s. (B) Linear plot for the voltammetric results of peptide sensor against (selected) SARS-CoV-2 SP concentrations ($n = 3$). (C) CV of BSA/NP/*b*/MB-GO/SPE electrodes against SARS-CoV-2 target protein (SP-I (1 pg/mL), SP-II (100 pg/mL)), interferents (NS1-I (100 pg/mL), NS1-II (100 ng/mL)), (HSA-I (100 pg/mL), HSA-II (100 ng/mL)), (IgG-I (100 pg/mL), IgG-II (100 ng/mL)) and mixture of target and interferents recorded in 0.1 M PBS (pH 7.4) at a scan rate of 50 mV/s. (D) Relative voltammetric histogram for the selectivity test against the target, interferents and mixture of target and interferents ($n = 3$).

electrode. It can be observed that the CA results enabled a concentration-dependent quenching with a wide linearity of studied SP concentrations (0.001 – 1000 ng/mL) (Fig. 4A). Although the current response of the BSA/NP/*b*/MB-GO/SPE electrode was nearly identical from 3 to 50 s, the variations are more visible around 50 s and therefore it was accounted for calibration. The linear fit for CA study is shown in Fig. 4B (circle trace). The sensitivity and the correlation coefficient obtained from the calibration plot was found to be 0.45 nA/pg mL^{-1} and 0.95, respectively. Selective bioaffinity of the immobilized bioreceptor was further validated using a scrambled NP region on the sensor platform. Distinct from the active NP region, the scrambled bioreceptor doesn't exhibit distinguishable variations in the amperogram derived current with the target SP at the electrode interface, evidenced from the insignificant correlation coefficient determination ($R^2 = 0.64$) (Fig. 4B, square trace). For instance, the current observed at 1 pg/mL and 10 pg/mL of target SP on sensor platform is merely equal. Similarly, the current response for analytes of 100 pg/mL, 1 ng/mL and 10 ng/mL exhibit insignificant output. Whereas the similar concentration in the test samples with the customized probe has distinguishable current response with respect to concentration. From which it is obvious that the developed sensor immobilized with active N-terminal region is exerting the selectivity against the SARS-CoV-2 SP. This is in agreement with CV studies compared with different layered peptide sensor platform (Fig. S8).

The LOD of target SP from CA study estimated to be 0.71 pg/mL using the above Eq. (1). As-prepared BSA/NP/*b*/MB-GO/SPE electrode system was also tested for cross-reactivity against the interferents (NS1, IgG, and HSA) (Fig. 4C). Observed chronoamperometric response denotes that the prepared peptide biosensor platform exhibits selective affinity toward the target SP protein (1 pg/mL and 100 pg/mL), while exert negligible response with the interferents (100 pg/mL and 100 ng/mL). Those results are presented in Fig. 4D and Table S6.

For the clinical proof-of-concept, COVID-19 positive human oro- and naso-pharyngeal swab samples (stored at ICMR-NIRT, Chennai, India) were utilized in the study. For negative control healthy volunteers' mouth gargled lavage samples were utilized. All the clinical validation studies were performed at ICMR-NIRT laboratory, Chennai. The oro- and naso-pharyngeal swab samples with varied cycle threshold (CT) values, validated by RT-PCR, were used to assess the clinical diagnostic feasibility of the peptide-based biosensor, as shown in Table S7. It's worth noting that RT-PCR is the gold standard technique for diagnosing COVID-19, which is based on detecting viral RNA from SARS-CoV-2 and is utilized here to assess sample viral loading, with higher CT indicating lower viral loading and lower CT indicating higher viral loading. Distinctly, the present peptide-based approach is to detect the SP from untreated swab samples rather than isolated RNA. Although RT-PCR results cannot be directly compared to developed biosensor platform, it provides unequivocal evidence of analytical performance. Fig. 4E and F demonstrates the biosensor response against the selected positive and negative samples, with respect to viral loads. Unlike other detection

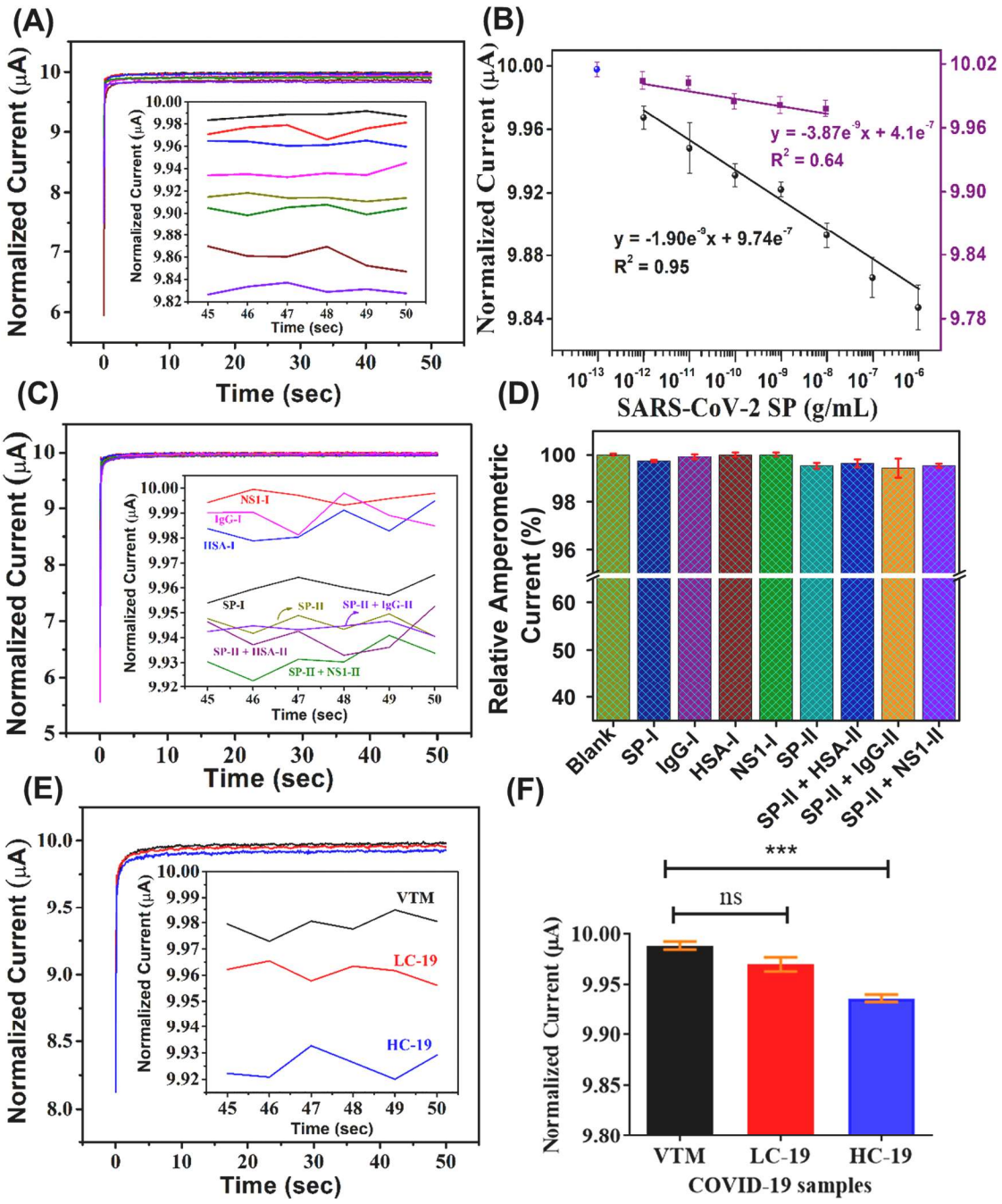

Fig. 4. (A) Chronoamperometric response of BSA/NP/*b*/MB-GO/SPE electrodes versus various concentrations of SARS-CoV-2 SP (inset a-h): 0, 0.001, 0.01, 0.1, 1, 10, 100 and 1000 ng/mL recorded in 0.1 M PBS (pH 7.4). Inset image represents the magnified normalized current response up to 50 s (B) Linear plot for the CA results of sensor platform with bio-active N-terminal region (circle trace) and scrambled N-terminal region (square trace) as bioreceptor against target SARS-CoV-2 SP ($n = 3$). Blue trace indicates the data point for the active N-terminal-modified electrode without target sample. (C) CA response of BSA/NP/*b*/MB-GO/SPE electrodes against SARS-CoV-2 target protein (SP-I (1 pg/mL), SP-II (100 pg/mL)), interferents (NS1-I (100 pg/mL), NS1-II (100 ng/mL)), (HSA-I (100 pg/mL), HSA-II (100 ng/mL)), (IgG-I (100 pg/mL), IgG-II (100 ng/mL)) and mixture of target and interferents recorded in 0.1 M PBS (pH 7.4). Inset image represents the magnified normalized current response up to 50 s (D) Relative amperometric histogram for the selectivity test against the target, interferents and mixture of target and interferents (n = 3). (E) Chronoamperometric response of BSA/NP/*b*/MB-GO/SPE electrodes against blank VTM, clinical samples (less SARS-CoV-2 (LC-19) and high SARS-CoV-2 (HC-19) infected human oropharyngeal and nasopharyngeal swab samples collected in VTM), respectively. Inset image represents the magnified normalized current response up to 50 s (F) Chronoamperometric histogram from of BSA/NP/*b*/MB-GO/SPE electrodes for clinical samples ($n = 3$). Statistical analyses were calculated using unpaired '*t*' test with Welsh's correction (*ns*: not statistically significant; *** $p < 0.005$).

approach, the customized N-terminal *h*ACE-2 associated peptides as bioreceptor exert a specificity toward the SP of SARS-CoV-2 without additional lysis or RNA isolation. As can be seen the current response measured from prepared biosensor platform exhibit a significant difference between the VTM and HC-19. The relevant % recovery calculated from CA studies are presented in Table S8.

CA results measured for artificially spiked target SP in gargled-lavage samples are presented in Figs. S9 and S10. All the measurements were done after 50 s of modifying the test sample on electrode surface. The histogram of normalized current implying the concentration-dependent

distinctness, which can be correlated with the target specific interaction mediated by customized N-terminal *h*ACE-2 probe peptides with the RBD regions of the SP. To investigate the stability of the prepared electrodes, CA measurements were performed in the weeks 0, 1, 2, 3, 4 and 5 (Fig. S11a). During this study, the fabricated peptide sensors were stored at 4–8 ºC. After 5th weeks of storage, the responsiveness of prepared peptide sensors was merely decreased (~0.41%) (Fig. S11b), enabling an acceptable sensitivity for long-term storage and analysis. The reproducibility of the peptide sensor was also investigated by fabricating three independently prepared substrates and tested for detecting a low concentration of analyte SP (0.1 ng/mL) and the relative standard deviation (RSD) was found to be 0.38%. Compared to conventional techniques, the electrochemical approach demonstrated herein is rapid and efficient without the need of isolation and amplification, viable for early identification of viral loads. With portable electrochemical workstation (Fig. S12), the demonstrated disposable electrode design and peptide-based SARS-CoV-2 SP detection is convenient for point-of-need analysis.

4. Conclusions

The present works demonstrates the application of customized N-terminal region of *h*ACE-2 associated synthetic oligopeptides as bioreceptor to design MB-GO electrochemical biosensor for targeting RBD of SARS-CoV-2. Activation of AnteoBind™ molecular glue on MB-GO sensor surface enabled better loading of bioreceptor on the disposable screen-printed electrodes, thus greatly simplifying the selectivity/specificity of the sensing system. Inherent redox behavior of MB ↔ LMB from the MB-GO sensor substrate were selectively influenced by the molecular interaction mediated from oligopeptides and RBD of SARS-CoV-2, irrespective of common interferents. While multiple testing strategies being demonstrated for SARS-CoV-2 analysis, peptide-based electrochemical biosensor platform is first of this kind exerting distinguishable signal with high sensitivity. The clinical feasibility of the prepared system, demonstrated with open source potentiostat, has the potential for resource limited settings due to its versatile analytical capability of oro- and naso-pharyngeal samples without additional reagents/treatment at less than a minute. Stability of the prepared sensor platform further warrants their customization in testing the other SARS-CoV-2 variants of interest and concern.

CRediT authorship contribution statement

T.H. Vignesh Kumar: Methodology, Formal analysis, Data curation, Validation, Writing – original draft. **Sowmiya Srinivasan**: Formal analysis, Data curation. **Vinoth Krishnan:** Validation, Formal analysis, Investigation, Data curation. **Rama Vaidyanathan**: Supervision, Project administration. **Kannadasan Anand Babu:** Methodology, Validation, Resources, Writing – review & editing. **Sudhakar Natarajan:** Methodology, Validation, Resources, Writing – review & editing. **Murugan Veerapandian:** Conceptualization, Funding acquisition, Methodology, Project administration, Supervision, Writing – review & editing.

Declaration of Competing Interest

The authors declare that they have no known competing financial interests or personal relationships that could have appeared to influence the work reported in this paper.

Data availability

Data will be made available on request.

Acknowledgments

Authors acknowledge the financial support from the Department of Biotechnology, File No. BT/PR40266/COD/139/2/2020, Government of India. This work was also supported by SERB, ASEAN-India Collaborative research project (CRD/2021/000451). Authors would like to thank Dr. Luke Elizabeth Hanna, Scientist 'F' and Head – Department of Virology and Biotechnology, ICMR- NIRT, Chennai for laboratory support. Authors would also like to acknowledge the staffs of Central Instrumentation Facility (CIF), CSIR-Central Electrochemical Research Institute, Karaikudi. CSIR-CECRI Manuscript Communication Number: CECRI/PESVC/Pubs/2022–030.

Appendix A. Supplementary material

Supplementary data associated with this article can be found in the online version at doi:10.1016/j.snb.2022.133052.

References

[1] Dashboard, WHO Coronavirus (COVID-19), World Health Organization, 2022. ⟨https://covid19.who.int/⟩.
[2] B. Hu, H. Guo, P. Zhou, Z.-L. Shi, Characteristics of SARS-CoV-2 and COVID-19, Nat. Rev. Microbiol. 19 (2021) 141–154, https://doi.org/10.1038/s41579-020-00459-7.
[3] H. Yang, Z. Rao, Structural biology of SARS-CoV-2 and implications for therapeutic development, Nat. Rev. Microbiol. 19 (2021) 685–700, https://doi.org/10.1038/s41579-021-00630-8.
[4] G. Mariano, R.J. Farthing, S.L.M. Lale-Farjat, J.R.C. Bergeron, Structural characterization of SARS-CoV-2: where we are, and where we need to be, Front. Mol. Biosci. (2020) 344, https://doi.org/10.3389/fmolb.2020.605236.
[5] J. Yang, S.J.L. Petitjean, M. Koehler, Q. Zhang, A.C. Dumitru, W. Chen, S. Derclaye, S.P. Vincent, P. Soumillion, D. Alsteens, Molecular interaction and inhibition of SARS-CoV-2 binding to the ACE2 receptor, Nat. Commun. 11 (2020) 4541, https://doi.org/10.1038/s41467-020-18319-6.
[6] M.A. Shereen, S. Khan, A. Kazmi, N. Bashir, R. Siddique, COVID-19 infection: emergence, transmission, and characteristics of human coronaviruses, J. Adv. Res. 24 (2020) 91–98, https://doi.org/10.1016/j.jare.2020.03.005.
[7] Y.-S. Chung, N.-J. Lee, S.H. Woo, J.-M. Kim, H.M. Kim, H.J. Jo, Y.E. Park, M.-G. Han, Validation of real-time RT-PCR for detection of SARS-CoV-2 in the early stages of the COVID-19 outbreak in the Republic of Korea, Sci. Rep. 11 (2021) 14817, https://doi.org/10.1038/s41598-021-94196-3.
[8] B.D. Kevadiya, J. Machhi, J. Herskovitz, M.D. Oleynikov, W.R. Blomberg, N. Bajwa, D. Soni, S. Das, M. Hasan, M. Patel, A.M. Senan, S. Gorantla, J. McMillan, B. Edagwa, R. Eisenberg, C.B. Gurumurthy, S.P.M. Reid, C. Punyadeera, L. Chang, H.E. Gendelman, Diagnostics for SARS-CoV-2 infections, Nat. Mater. 20 (2021) 593–605, https://doi.org/10.1038/s41563-020-00906-z.
[9] T.C. Kwee, R.M. Kwee, Chest CT in COVID-19: what the radiologist needs to know, RadioGraphics 40 (2020) 1848–1865, https://doi.org/10.1148/rg.2020200159.
[10] X. Li, W. Zeng, X. Li, H. Chen, L. Shi, X. Li, H. Xiang, Y. Cao, H. Chen, C. Liu, J. Wang, CT imaging changes of corona virus disease 2019(COVID-19): a multi-center study in Southwest China, J. Transl. Med. 18 (2020) 154, https://doi.org/10.1186/s12967-020-02324-w.
[11] X. Wang, C. Liu, L. Hong, C. Yuan, J. Ding, Q. Jia, G. Sun, W. Peng, Q. Sun, CT findings of patients infected with SARS-CoV-2, BMC Med. Imaging 20 (2020) 70, https://doi.org/10.1186/s12880-020-00471-6.
[12] C. Chaimayo, B. Kaewnaphan, N. Tanlieng, N. Athipanyasilp, R. Sirijatuphat, M. Chayakulkeeree, N. Angkasekwinai, R. Sutthent, N. Puangpunngam, T. Tharmviboonsri, O. Pongraweewan, S. Chuthapisith, Y. Sirivatanauksorn, W. Kantakamalakul, N. Horthongkham, Rapid SARS-CoV-2 antigen detection assay in comparison with real-time RT-PCR assay for laboratory diagnosis of COVID-19 in Thailand, Virol. J. 17 (2020) 177, https://doi.org/10.1186/s12985-020-01452-5.
[13] I. Dorigatti, E. Lavezzo, L. Manuto, C. Ciavarella, M. Pacenti, C. Boldrin, M. Cattai, F. Saluzzo, E. Franchin, C. Del Vecchio, F. Caldart, G. Castelli, M. Nicoletti, E. Nieddu, E. Salvadoretti, B. Labella, L. Fava, S. Guglielmo, M. Fascina, M. Grazioli, G. Alvisi, M.C. Vanuzzo, T. Zupo, R. Calandrin, V. Lisi, L. Rossi, I. Castagliuolo, S. Merigliano, H.J.T. Unwin, M. Plebani, A. Padoan, A.R. Brazzale, S. Toppo, N.M. Ferguson, C.A. Donnelly, A. Crisanti, SARS-CoV-2 antibody dynamics and transmission from community-wide serological testing in the Italian municipality of Vo', Nat. Commun. 12 (2021) 4383, https://doi.org/10.1038/s41467-021-24622-7.
[14] A. García-Miranda Ferrari, S.J. Rowley-Neale, C.E. Banks, Screen-printed electrodes: transitioning the laboratory in-to-the field, Talanta Open 3 (2021), 100032, https://doi.org/10.1016/j.talo.2021.100032.
[15] C.I.L. Justino, A.R. Gomes, A.C. Freitas, A.C. Duarte, T.A.P. Rocha-Santos, Graphene based sensors and biosensors, TrAC Trends Anal. Chem. 91 (2017) 53–66, https://doi.org/10.1016/j.trac.2017.04.003.
[16] A.T. Lawal, Progress in utilisation of graphene for electrochemical biosensors, Biosens. Bioelectron. 106 (2018) 149–178, https://doi.org/10.1016/j.bios.2018.01.030.
[17] A.T. Lawal, Graphene-based nano composites and their applications. A review, Biosens. Bioelectron. 141 (2019), 111384, https://doi.org/10.1016/j.bios.2019.111384.

[18] P. Kanagavalli, C. Andrew, M. Veerapandian, M. Jayakumar, In-situ redox-active hybrid graphene platform for label-free electrochemical biosensor: Insights from electrodeposition and electroless deposition, TrAC Trends Anal. Chem. 143 (2021), 116413, https://doi.org/10.1016/j.trac.2021.116413.

[19] W. Daniel, W. Nianshuang, K.S. Corbett, J.A. Goldsmith, C.-L. Hsieh, O. Abiona, B. S. Graham, J.S. McLellan, Cryo-EM structure of the 2019-nCoV spike in the prefusion conformation, Science 367 (6483) (2020) 1260–1263, https://doi.org/10.1126/science.abb2507.

[20] H. Heike, P. Krzysztof, van der H. Lia, G. Martina, B. Ben, P. Stefan, Human coronavirus NL63 employs the severe acute respiratory syndrome coronavirus receptor for cellular entry, Proc. Natl. Acad. Sci. 102 (2005) 7988–7993, https://doi.org/10.1073/pnas.0409465102.

[21] W. Li, M.J. Moore, N. Vasllieva, J. Sui, S.K. Wong, M.A. Berne, M. Somasundaran, J.L. Sullivan, K. Luzuriaga, T.C. Greeneugh, H. Choe, M. Farzan, Angiotensin-converting enzyme 2 is a functional receptor for the SARS coronavirus, Nature 426 (2003) 450–454, https://doi.org/10.1038/nature02145.

[22] E.M. Bressler, J. Kim, R.B. Shmueli, A.C. Mirando, H. Bazzazi, E. Lee, A.S. Popel, N. B. Pandey, J.J. Green, Biomimetic peptide display from a polymeric nanoparticle surface for targeting and antitumor activity to human triple-negative breast cancer cells, J. Biomed. Mater. Res. Part A 106 (2018) 1753–1764, https://doi.org/10.1002/jbm.a.36360.

[23] R. Ling, Y. Dai, B. Huang, W. Huang, J. Yu, X. Lu, Y. Jiang, In silico design of antiviral peptides targeting the spike protein of SARS-CoV-2, Peptides 130 (2020), 170328, https://doi.org/10.1016/j.peptides.2020.170328.

[24] Y. Han, P. Král, Computational design of ACE2-based peptide inhibitors of SARS-CoV-2, ACS Nano 14 (2020) 5143–5147, https://doi.org/10.1021/acsnano.0c02857.

[25] G. Zhang, S. Pomplun, A.R. Loftis, A. Loas, B.L. Pentelute, The first-in-class peptide binder to the SARS-CoV-2 spike protein, BioRxiv (2020), https://doi.org/10.1101/2020.03.19.999318.

[26] T.W. Linsky, R. Vergara, N. Codina, J.W. Nelson, M.J. Walker, W. Su, C.O. Barnes, T.-Y. Hsiang, K. Esser-Nobis, K. Yu, De novo design of potent and resilient hACE2 decoys to neutralize SARS-CoV-2, Science 370 (6521) (2020) 1208–1214, https://doi.org/10.1126/science.abe0075.

[27] Q. Zhu, X. Zhou, A colorimetric sandwich-type bioassay for SARS-CoV-2 using a hACE2-based affinity peptide pair, J. Hazard Mater. 425 (2022), 127923, https://doi.org/10.1016/j.jhazmat.2021.127923.

[28] Y. Lai, G. Fois, J.R. Flores, M.J. Tuvim, Q. Zhou, K. Yang, J. Leitz, J. Peters, Y. Zhang, R.A. Pfuetzner, Inhibition of calcium-triggered secretion by hydrocarbon-stapled peptides, Nature (2022) 1–8, https://doi.org/10.1038/s41586-022-04543-1.

[29] J.-D. Malcor, D. Bax, S.W. Hamaia, N. Davidenko, S.M. Best, R.E. Cameron, R. W. Farndale, D. Bihan, The synthesis and coupling of photoreactive collagen-based peptides to restore integrin reactivity to an inert substrate, chemically-crosslinked collagen, Biomaterials 85 (2016) 65–77, https://doi.org/10.1016/j.biomaterials.2016.01.044.

[30] C. di Natale, E. Battista, V. Lettera, N. Reddy, G. Pitingolo, R. Vecchione, F. Causa, P.A. Netti, Easy surface functionalization and bioconjugation of peptides as capture agents of a microfluidic biosensing platform for multiplex assay in serum, Bioconjug. Chem. 32 (2021) 1593–1601, https://doi.org/10.1021/acs.bioconjchem.1c00146.

[31] Y. Li, D. Lai, S. Tao, SARS-CoV-2 spike linear epitope scanning via a peptide microarray through sera profiling, STAR Protoc. 2 (2021), 100707, https://doi.org/10.1016/j.xpro.2021.100707.

[32] H. Andresen, C. Grötzinger, K. Zarse, M. Birringer, C. Hessenius, O.J. Kreuzer, E. Ehrentreich-Förster, F.F. Bier, Peptide microarrays with site-specifically immobilized synthetic peptides for antibody diagnostics, Sens Actuators B Chem. 113 (2006) 655–663, https://doi.org/10.1016/j.snb.2005.07.033.

[33] A. McQuistan, A.J. Zaitouna, E. Echeverria, R.Y. Lai, Use of thiolated oligonucleotides as anti-fouling diluents in electrochemical peptide-based sensors, Chem. Commun. 50 (2014) 4690–4692, https://doi.org/10.1039/C4CC01290A.

[34] E. Farkas, R. Tarr, T. Gerecsei, A. Saftics, K.D. Kovács, B. Stercz, J. Domokos, B. Peter, S. Kurunczi, I. Szekacs, Development and in-depth characterization of bacteria repellent and bacteria adhesive antibody-coated surfaces using optical waveguide biosensing, Biosensors 12 (2022) 56, https://doi.org/10.3390/bios12020056.

[35] P. Kanagavalli, M. Veerapandian, Opto-electrochemical functionality of Ru(II)-reinforced graphene oxide nanosheets for immunosensing of dengue virus non-structural 1 protein, Biosens. Bioelectron. 150 (2020), 111878, https://doi.org/10.1016/j.bios.2019.111878.

[36] P. Karoyan, V. Vieillard, L. Gómez-Morales, E. Odile, A. Guihot, C.-E. Luyt, A. Denis, P. Grondin, O. Lequin, Human ACE2 peptide-mimics block SARS-CoV-2 pulmonary cells infection, Commun. Biol. 4 (2021) 197, https://doi.org/10.1038/s42003-021-01736-8.

[37] S. Yang, D. Liu, Q.B. Meng, S. Wu, X.-M. Song, Reduced graphene oxide-supported methylene blue nanocomposite as a glucose oxidase-mimetic for electrochemical glucose sensing, RSC Adv. 8 (2018) 32565–32573, https://doi.org/10.1039/C8RA06208K.

[38] M. Veerapandian, R. Hunter, S. Neethirajan, Dual immunosensor based on methylene blue-electroadsorbed graphene oxide for rapid detection of the influenza A virus antigen, Talanta 155 (2016) 250–257, https://doi.org/10.1016/j.talanta.2016.04.047.

[39] S. Saxena, T.A. Tyson, S. Shukla, E. Negusse, H. Chen, J. Bai, Investigation of structural and electronic properties of graphene oxide, Appl. Phys. Lett. 99 (2011) 13104, https://doi.org/10.1063/1.3607305.

[40] S. Perumbilavil, P. Sankar, T. Priya Rose, R. Philip, White light Z-scan measurements of ultrafast optical nonlinearity in reduced graphene oxide nanosheets in the 400–700 nm region, Appl. Phys. Lett. 107 (2015) 51104, https://doi.org/10.1063/1.4928124.

[41] C. Li, Y. Huang, K. Lai, B.A. Rasco, Y. Fan, Analysis of trace methylene blue in fish muscles using ultra-sensitive surface-enhanced Raman spectroscopy, Food Control 65 (2016) 99–105, https://doi.org/10.1016/j.foodcont.2016.01.017.

[42] A. Eckmann, A. Felten, A. Mishchenko, L. Britnell, R. Krupke, K.S. Novoselov, C. Casiraghi, Probing the nature of defects in graphene by Raman spectroscopy, Nano Lett. 12 (2012) 3925–3930, https://doi.org/10.1021/nl300901a.

[43] R. Abdel-Hamid, A. Bakr, E.F. Newair, F. Garcia, Simultaneous voltammetric determination of gallic and protocatechuic acids in mango juice using a reduced graphene oxide-based electrochemical sensor, Beverages 5 (2019), https://doi.org/10.3390/beverages5010017.

[44] T.H.V. Kumar, A.K. Sundramoorthy, Non-enzymatic electrochemical detection of urea on silver nanoparticles anchored nitrogen-doped single-walled carbon nanotube modified electrode, J. Electrochem. Soc. 165 (2018) B3006–B3016, https://doi.org/10.1149/2.0021808jes.

[45] Y. Yan, M. Zhang, K. Gong, L. Su, Z. Guo, L. Mao, Adsorption of methylene blue dye onto carbon nanotubes: a route to an electrochemically functional nanostructure and its layer-by-layer assembled nanocomposite, Chem. Mater. 17 (2005) 3457–3463, https://doi.org/10.1021/cm0504182.

[46] D. Zhang, L. Fu, L. Liao, N. Liu, B. Dai, C. Zhang, Preparation, characterization, and application of electrochemically functional graphene nanocomposites by one-step liquid-phase exfoliation of natural flake graphite with methylene blue, Nano Res. 5 (2012) 875–887, https://doi.org/10.1007/s12274-012-0271-9.

[47] D. Zhang, X. Ouyang, W. Ma, L. Li, Y. Zhang, Voltammetric determination of folic acid using adsorption of methylene blue onto electrodeposited of reduced graphene oxide film modified glassy carbon electrode, Electroanalysis 28 (2016) 312–319, https://doi.org/10.1002/elan.201500348.

[48] H. Liu, R. Malhotra, M.W. Peczuh, J.F. Rusling, Electrochemical immunosensors for antibodies to peanut allergen Ara h2 using gold nanoparticle– peptide films, Anal. Chem. 82 (2010) 5865–5871, https://pubs.acs.org/doi/10.1021/ac101110q.

[49] V. Vanova, K. Mitrevska, V. Milosavljevic, D. Hynek, L. Richtera, V. Adam, Peptide-based electrochemical biosensors utilized for protein detection, Biosens. Bioelectron. 180 (2021), 113087, https://doi.org/10.1016/j.bios.2021.113087.

[50] J.H. Kim, C.H. Cho, M.Y. Ryu, J.-G. Kim, S.-J. Lee, T.J. Park, J.P. Park, Development of peptide biosensor for the detection of dengue fever biomarker, nonstructural 1, e0222144, PLoS One 14 (2019), https://doi.org/10.1371/journal.pone.0222144.

[51] D.P. Valencia, L.M.F. Dantas, A. Lara, J. García, Z. Rivera, J. Rosas, M. Bertotti, Development of a bio-electrochemical immunosensor based on the immobilization of SPINNTKPHEAR peptide derived from HPV-L1 protein on a gold electrode surface, J. Electroanal. Chem. 770 (2016) 50–55, https://doi.org/10.1016/j.jelechem.2016.03.040.

[52] M. Puiu, A. Idili, D. Moscone, F. Ricci, C. Bala, A modular electrochemical peptide-based sensor for antibody detection, Chem. Commun. 50 (2014) 8962–8965, https://doi.org/10.1039/C4CC02858A.

[53] H. Li, Y. Cao, X. Wu, Z. Ye, G. Li, Peptide-based electrochemical biosensor for amyloid β 1–42 soluble oligomer assay, Talanta 93 (2012) 358–363, https://doi.org/10.1016/j.talanta.2012.02.055.

[54] B. Tian, F. Gao, J. Fock, M. Dufva, M.F. Hansen, Homogeneous circle-to-circle amplification for real-time optomagnetic detection of SARS-CoV-2 RdRp coding sequence, Biosens. Bioelectron. 165 (2020), 112356, https://doi.org/10.1016/j.bios.2020.112356.

[55] M. Patchsung, K. Jantarug, A. Pattama, K. Aphicho, S. Suraritdechachai, P. Meesawat, K. Sappakhaw, N. Leelahakorn, T. Ruenkam, T. Wongsatit, N. Athipanyasilp, B. Eiamthong, B. Lakkanasirorat, T. Phoodokmai, N. Niljianskul, D. Pakotiprapha, S. Chanarat, A. Homchan, R. Tinikul, P. Kamutira, K. Phiwkaow, S. Soithongcharoen, C. Kantiwiriyawanitch, V. Pongsupasa, D. Trisrivirat, J. Jaroensuk, T. Wongnate, S. Maenpuen, P. Chaiyen, S. Kamnerdnakta, J. Swangsri, S. Chuthapisith, Y. Sirivatanauksorn, C. Chaimayo, R. Sutthent, W. Kantakamalakul, J. Joung, A. Ladha, X. Jin, J.S. Gootenberg, O.O. Abudayyeh, F. Zhang, N. Horthongkham, C. Uttamapinant, Clinical validation of a Cas13-based assay for the detection of SARS-CoV-2 RNA, Nat. Biomed. Eng. 4 (2020) 1140–1149, https://doi.org/10.1038/s41551-020-00603-x.

[56] T. Chaibun, J. Puenpa, T. Ngamdee, N. Boonapatcharoen, P. Athamanolap, A. P. O'Mullane, S. Vongpunsawad, Y. Poovorawan, S.Y. Lee, B. Lertanantawong, Rapid electrochemical detection of coronavirus SARS-CoV-2, Nat. Commun. 12 (2021) 802, https://doi.org/10.1038/s41467-021-21121-7.

[57] J. Jiao, C. Duan, L. Xue, Y. Liu, W. Sun, Y. Xiang, DNA nanoscaffold-based SARS-CoV-2 detection for COVID-19 diagnosis, Biosens. Bioelectron. 167 (2020), 112479, https://doi.org/10.1016/j.bios.2020.112479.

[58] L. Kashefi-Kheyrabadi, H.V. Nguyen, A. Go, C. Baek, N. Jang, J.M. Lee, N.-H. Cho, J. Min, M.-H. Lee, Rapid, multiplexed, and nucleic acid amplification-free detection of SARS-CoV-2 RNA using an electrochemical biosensor, Biosens. Bioelectron. 195 (2022), 113649, https://doi.org/10.1016/j.bios.2021.113649.

[59] H.E. Kim, A. Schuck, S.H. Lee, Y. Lee, M. Kang, Y.-S. Kim, Sensitive electrochemical biosensor combined with isothermal amplification for point-of-care COVID-19

tests, Biosens. Bioelectron. 182 (2021), 113168, https://doi.org/10.1016/j.bios.2021.113168.
[60] H. Zhao, F. Liu, W. Xie, T.-C. Zhou, J. OuYang, L. Jin, H. Li, C.-Y. Zhao, L. Zhang, J. Wei, Y.-P. Zhang, C.-P. Li, Ultrasensitive supersandwich-type electrochemical sensor for SARS-CoV-2 from the infected COVID-19 patients using a smartphone, Sens Actuators B Chem. 327 (2021), 128899, https://doi.org/10.1016/j.snb.2020.128899.
[61] L. Liv, G. Çoban, N. Nakiboğlu, T. Kocagöz, A rapid, ultrasensitive voltammetric biosensor for determining SARS-CoV-2 spike protein in real samples, Biosens. Bioelectron. 192 (2021), 113497, https://doi.org/10.1016/j.bios.2021.113497.

Dr. T.H. Vignesh Kumar is a Post-Doctoral Research Associate in the Electrical and Computer Engineering, Iowa State University, USA since January 2022. He received his Ph.D. degree in Chemistry from the SRM Institute of Science and Technology, Chennai, India, in 2021. He was a Senior Project Associate at the Electrodics and Electrocatalysis Division (EEC), CSIR-CECRI, India, from December 2020 to May 2021. He was a Post-Doctoral Fellow at the School of Medical Science and Technology, IIT Kharagpur, India, from August 2021 to December 2021. His research interests span around chemical and biosensors, flexible electrodes, transistors, materials chemistry, electroanalysis and biomaterials.

Ms. Sowmiya Srinivasan is a Junior Executive in Acrannolife Genomics Pvt. Ltd., Chennai since May 2021. She was graduated in 2020 with Master of Technology (Biotechnology) from PSG College of Technology, Coimbatore. Her research interests include recombinant protein expression and developing diagnostic method for infectious diseases.

Mr. Vinoth Krishnan is an AcSIR Ph.D., scholar in Electrodics and Electrocatalysis Division (EEC), CSIR-CECRI. He completed his undergraduate in Chemistry (2017) from Bishop Heber College, Trichy, and obtained a postgraduate degree (2019) in General Chemistry from Manonmaniam Sundaranar University, Tirunelveli, Tamil Nadu. His research interests include biofunctionalized materials for opto-electrochemical studies, construction of sensor platform for clinically important biomarkers, and synthesis of redox-active phytochemical compounds, in addition to point-of-care diganostic development.

Dr. Rama Vaidyanathan is a Professor of Biotechnology in Dr APJ Abdul Kalam Center of Excellence in Innovation and Entrepreneurship, Dr. MGR Educational and Research Institute, India since 2005. She completed her Ph.D. in 1998 in Plant Molecular Biology from SPIC Science Foundation, Chennai, Tamil Nadu, India and her post-doctoral research in School of Biology, University of California, San Diego, USA. Her present research interests include mechanisms of antibiotic resistance in Klebsiella pneumoniae, whole genome analysis in bacteria and the study of biodiversity of mosquitoes in India. She is also a trained entrepreneurship educator.

Dr. Kannadasan Anand Babu is a Research Scientist in Dr. APJ Abdul Kalam Center of Excellence in Innovation and Entrepreneurship, Dr. MGR Educational and Research Institute, India since 2019. He did his Ph.D., (2020) in Biochemistry and Cell Biology (Biotechnology) from SASTRA University, India. His research interests include identifying novel biomarkers for the systemic illness and environmental pollution control. He is also working on the active constituents from phytochemical for obesity induced oxidative stress in animal model.

Dr. Sudhakar Natarajan is a Scientist in Department of Virology and Biotechnology, National Institute for Research in Tuberculosis, ICMR, India since Jan. 2018. He has done his doctoral work at Cancer Institute, Adyar, Chennai and received his Ph.D., (2008) in Molecular Biology and Molecular Oncology from University of Madras. He had a Post-doctoral stint at National Cancer Institute (NCI), Frederick, MD during 2007–2008. His research interest includes Molecular oncology, Molecular immunology, Tuberculosis & viral genomics and Transcriptomics, Molecular diagnostics, and Bioinformatics. He has developed and validated a diagnostic method for early detection of HPV infection in cervical cancer. He received grants from DST, DBT, SERB, and ICMR (Intramural), Govt. of India for his credit.

Dr. Murugan Veerapandian is a Scientist and an Assistant Professor of Biological Sciences in Electrodics and Electrocatalysis Division (EEC), CSIR-CECRI, India since 2017. He received Ph.D., (2013) in Biomedical Engineering (BioNanotechnology) from Gachon University, South Korea. He has been awarded with GRSTB Postdoctoral fellowship at Université de Montréal (2013–2015), QC. Afterward he pursued a second postdoctoral research at BioNano Lab, University of Guelph (2015–2016), ON, Canada. He was a DST-INSPIRE Faculty at NIPER-Kolkata (2016–2017), West Bengal, India. He led a Bio-MedNano research within EEC of CSIR-CECRI focused on development of electrochemical immuno-/geno-sensor platform for viral infection-associated marker's detection. Further, optimize redox-active phytochemical as active component for theranostics, antioxidant and biosensor application. He is also involved in the development of non-invasive and real-time assay of cell-drug interaction.